JOURNAL OF Applied Polymer SCIENCE

Layer Double Hydroxides for Enhanced Poly(3-hydroxybutyrate-*co*-3-hydroxyvalerate) Crystallization

Koffi L. Dagnon,[1,*] Clark Robinson,[1] Hua H. Chen,[1] David C. Garrett,[1] Lucia H. Innocentini-Mei,[2] Nandika A. D'Souza[1,3]

[1]Department of Materials Science and Engineering, University of North Texas, Denton, Texas 76203
[2]UNICAMP School of Chemical Engineering, State University of Campinas, Campina, São Paulo, Brazil
[3]Department of Mechanical and Energy Engineering, University of North Texas, Denton, Texas 76203
*Present address: Department of Macromolecular Science and Engineering, Case Western Reserve University, 2100 Adelbert Road, Cleveland, OH 44106, USA
Correspondence to: N. A. D'Souza (E-mail: ndsouza@unt.edu)

ABSTRACT: Enabling the widespread utilization of poly[(3-hydroxybutyrate)-*co*-(3-hydroxyvalerate)] (PHBV) is strongly associated with enhancing its crystallization kinetics. In this article, we utilize a highly surface active (one reactive group per nanometer square) anion exchanged layered-double hydroxide (LDH) functionalized by stearic acid to probe the crystallization kinetics of PHBV. Our prior work has shown that the addition of LDH decreases the cold crystallization and induces a melt recrystallization peak in PHBV. Since the melt-recrystallization temperature shifted to higher temperature and its corresponding enthalpy increased with increasing LDH loading, this article is focused on understanding the effect of LDH on kinetics and energetics of PHBV crystallization. Both Avrami and Lauritzen–Hoffman modeling are utilized to develop a comprehensive understanding of thermal history effects through differential scanning calorimetry and polarized optical microscopy measurements. Five concentrations by weight of LDH are used: 1, 3, 5, and 7%. The results show that the addition of LDH promoted both primary and secondary nucleation at low concentrations but additional LDH resulted in primary nucleation alone. The crystallization rate and activation energy show a significant increase, which is accompanied by a decrease in the nucleation constant, the surface energy and the work of chain folding for PHBV crystallization. © 2012 Wiley Periodicals, Inc. J Appl Polym Sci 000: 000–000, 2012

KEYWORDS: PHBV; layered-double hydroxides; crystallization kinetics; nanocomposites

Received 9 June 2010; accepted 8 February 2012; published online
DOI: 10.1002/app.37646

INTRODUCTION

Biopolymers have been extensively investigated from ecological and biomedical perspectives. As a consequence, many researchers are motivated to move towards materials that can be produced from renewable resources and would not remain in the environment after disposal.[1] Among them, poly(hydroxyalkanoic acid)s (PHAs), poly-lactic acid, thermoplastic starch, and their copolymers or blends with other biopolymers are attracting much interest. They represent a potential substitute to petroleum-based synthetic polymers. However, many biopolymers are expensive and exhibit inferior mechanical properties. When processed under conventional methods such as injection molding and extrusion, their slow crystallization rate leads to part tackiness and low-dimensional stability. There is thus a critical need to improve the crystallization rate of the biopolymers to make them fully competitive with conventional thermoplastics. One approach is to combine them with nano-sized fillers.[1] Many experimental studies have shown that incorporating nanoscale inclusions in a polymer-matrix results in significant improvement in mechanical, thermal, electrical, and other physical properties.[2]

PHAs are polyesters of hydroxyalkanoic acids synthesized by bacteria as intracellular-carbon and energy storage compounds and accumulated as granules in the cytoplasm of cells.[3] As biodegradable and biocompatible materials, they have attracted much attention in diverse applications.[4] A frequently utilized member of the PHAs family is poly(3-hydroxybutyrate) or P(3HB), a polymerized 3-hydroxybutyrate (3-HB) discovered in 1927 by Lemoigne. This biomaterial has distinct properties including biodegradability, biocompatibility, and piezoelectric

characteristics.[5] It also has the particular advantage that it is thermoplastic and therefore, in principle, can be processed using existing processing equipment. However, there are also many drawbacks to the use of P(3HB), mainly its tendency to be a rather brittle and stiff material when compared with common chemosynthesized plastics as well as its narrow processing window, limiting manufacturability.[3,6] These drawbacks prevent its practical application, and various copolyesters of P(3HB) have been developed to surmount these shortcomings. Frequently utilized copolyesters of P(3HB) include poly(3-hydroxybutyrate-*co*-3-hydroxyvalerate) or [P(3HB-*co*-3HV)], which is 3-hydroxyvalerate (3-HV) units polymerized with 3-HB units and poly(3-hydroxybutyrate-*co*-4-hydroxybutyrate) or [P(3HB-*co*-4HB)], which is a random copolymer of 4-hydroxybutyrate (4-HB) units with 3-HB units. With respect to the homopolyester P(3HB), these copolyesters are characterized by more desirable processing properties.[3,7] Molar fractions of 3-HV and 4-HB strongly affect the physical properties of P(3HB) copolyesters.[3,8]

The copolyester P(3HB-*co*-3HV) or PHBV presented in Scheme 1 is a semi-crystalline material, which is both biodegradable and biocompatible.[9] These properties make it attractive as a biomedical and environmentally friendly material. On the other hand, the application of PHBV is hindered by some disadvantages such as the development of interlamellar secondary crystallization on storage, slow crystallization rate, high brittleness, and high-production costs.[10] Its brittleness is due to the inherent defects in the big spherulites, whereas its low nucleation density is due to its high purity.[11] Therefore, the expansion of commercial applications for PHBV will necessitate the improvement of the crystallization and processing behavior, diminution of overall cost, improvement of the brittleness and enhancement of the mechanical properties.[12]

In addition, a large fraction of PHBV remains amorphous and slowly undergoes crystallization during storage.[13] Increased rate of crystallization of PHBV can be obtained by the addition of a small amount of nucleating agent. Ma et al.[11] and Chen et al.[14] studied the effect of nucleating agents such as fumed silica and silicate layers on the crystallization behavior of PHBV. A number of additives including thymine and melamine,[13] talc and boron nitride[15] have been also proposed to overcome the crystallization shortcomings of PHBV.

Our nucleating agent, layered-double hydroxides (LDHs) are synthetic clays[16] with a high-surface activity of one reactive site per nanometer square and have been increasingly investigated as additives in polymers.[17–21] The composition of LDHs may be generally represented by the ideal formula $[M^{2+}_{1-x}M^{3+}_{x}(OH)_2]^{x+}A^{n-}_{x/n}\cdot mH_2O$, where M^{2+} and M^{3+} are divalent and trivalent metal cations such as Zn^{2+}, Al^{3+}, respectively, *A* is an anion, such as NO^{3-}, CO_3^{2-}, SO_4^{2}. In general, modified LDHs can be prepared with simple procedures, at a high level of purity. They are cheap and eco-compatible and can be organically modified with different organic anions.

In this effort, we synthesize LDH based on Zn, Al in the ratio of 2 : 1 confirmed by elemental analysis.[21] We have previously reported on the substantial mechanical property improvement, wide angle X-ray diffraction (WAXD) and transmission electron microscopy (TEM) results of the intercalation of LDH, and nonisothermal differential scanning calorimetry (DSC) results of PHBV/LDH nanocomposites.[21] A relatively constant increase in d-spacing observed in our WAXD work, indicated that the nanocomposites were intercalated composites with limited to no exfoliation apparent in the TEM. The authors observed that neat biopolymer did not show any melt-recrystallization temperature (T_{mc}) upon cooling. However, with the addition of the nanofiller, PHBV exhibited a T_{mc} that shifter slightly to higher temperature and whose enthalpy of melt recrystallization showed a substantial increase with increased LDH concentration (10.8 J/g for 1 wt % LDH and 55.8 J/g for 7 wt % LDH). Since the critical need for PHBV is an increase in crystallization rate, the impact of LDH on the crystallization kinetics and energetics is the focus of this effort.

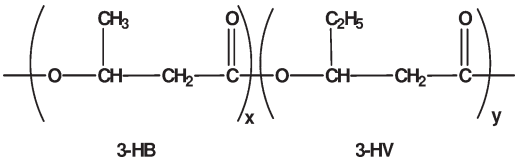

Scheme 1. Chemical structure of P(3HB-*co*-3HV) or PHBV.

The present study will present the nonisothermal crystallization behavior of PHBV, and PHBV/LDH nanocomposites using DSC and polarized optical microscopy (POM). An analysis of the crystallization kinetics and activation energy, making use of Avrami model and Arrhenius equation, respectively is conducted. It will also present an analysis of the spherulitic crystallization kinetics, making use of the Lauritzen–Hoffman theory of secondary nucleation.

EXPERIMENTAL

Materials

PHBV (M_w = 250,000–400,000 Da) with 18 mol% (3-HV) content was supplied by PHB Industrial, Sao Paol, Brazil and dried in oven for 48 h at 40°C. The Zn–Al nitrate LDH, organically modified with stearic acid or LDH represented by the formula Zn_2Al $(OH)_6$ $C_{18}H_{35}O_2$ was used as synthetic nanofiller. Its synthesis in our laboratory has been described previously.21 Chloroform (>99.8% purity, EMD Chemicals, Gibbstown, NJ) was used as received.

Preparation of the Intercalated Composites Films

Intercalated composites were fabricated by the solution-casting technique. Initially, LDH powder was dispersed in chloroform and stirred for 10 min. Then, PHBV powder was added and the mixture was heated at 56°C under vigorous stirring for 4 h. The resulting dispersion was allowed to age for 24 h. Nanocomposite films were prepared by spin casting (without any substrate needed on the custom-built spin caster) and the samples were dried under vacuum at 40°C for 4 days to remove residual solvent. They were then kept in a desiccator for experimental purposes. The LDH content of the fabricated films was 1, 3, 5, and 7 wt %. Samples, in this study are designated as PHBV/LDH*n*, where *n* is the amount of LDH used in the preparation of the intercalated composites. Two batches of each sample were

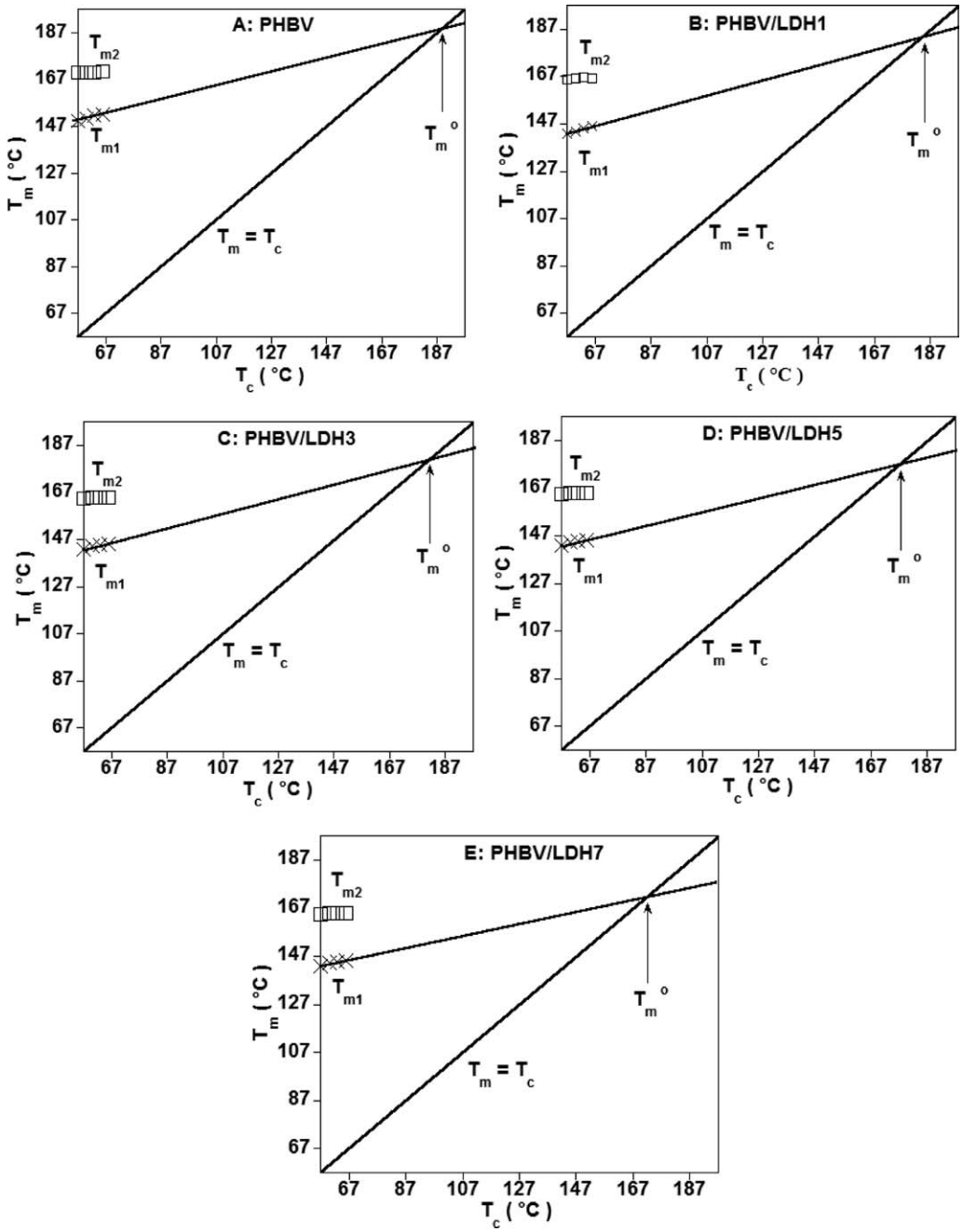

Figure 1. Plots of T_m as a function of T_c for neat PHBV and PHBV/LDH*n* nanocomposites.

prepared to establish reproducibility and measurements were conducted on each of them.

Differential Scanning Calorimetry Measurements

A Perkin-Elmer DSC-6 (Waltham, MA) was used to characterize the thermal transitions and to monitor the rate of heat flow from PHBV and PHBV/LDH*n* intercalated composites samples during isothermal crystallization from the melt. The instrument was calibrated with an indium standard. The measurement was conducted under a nitrogen atmosphere. The sample weight was kept in the 5–6 mg range.

The procedure for isothermal crystallization kinetic experiment was as follows: all samples were first heated from 25 to 190°C at 50°C min^{-1} and held at 190°C for 5 min to erase all prior thermal history. They were quenched to the chosen crystallization temperature, T_c, at 50°C min^{-1} and held at T_c for the crystallization process to occur. The exothermic crystallization peak was recorded as a function of time at T_c. The heat generated during the development of the crystalline phase was recorded up to a vanishing-thermal effect and analyzed according to the usual procedure to obtain the relative degree of crystallinity at time t, X_{rel} [eq. (1)].[15]

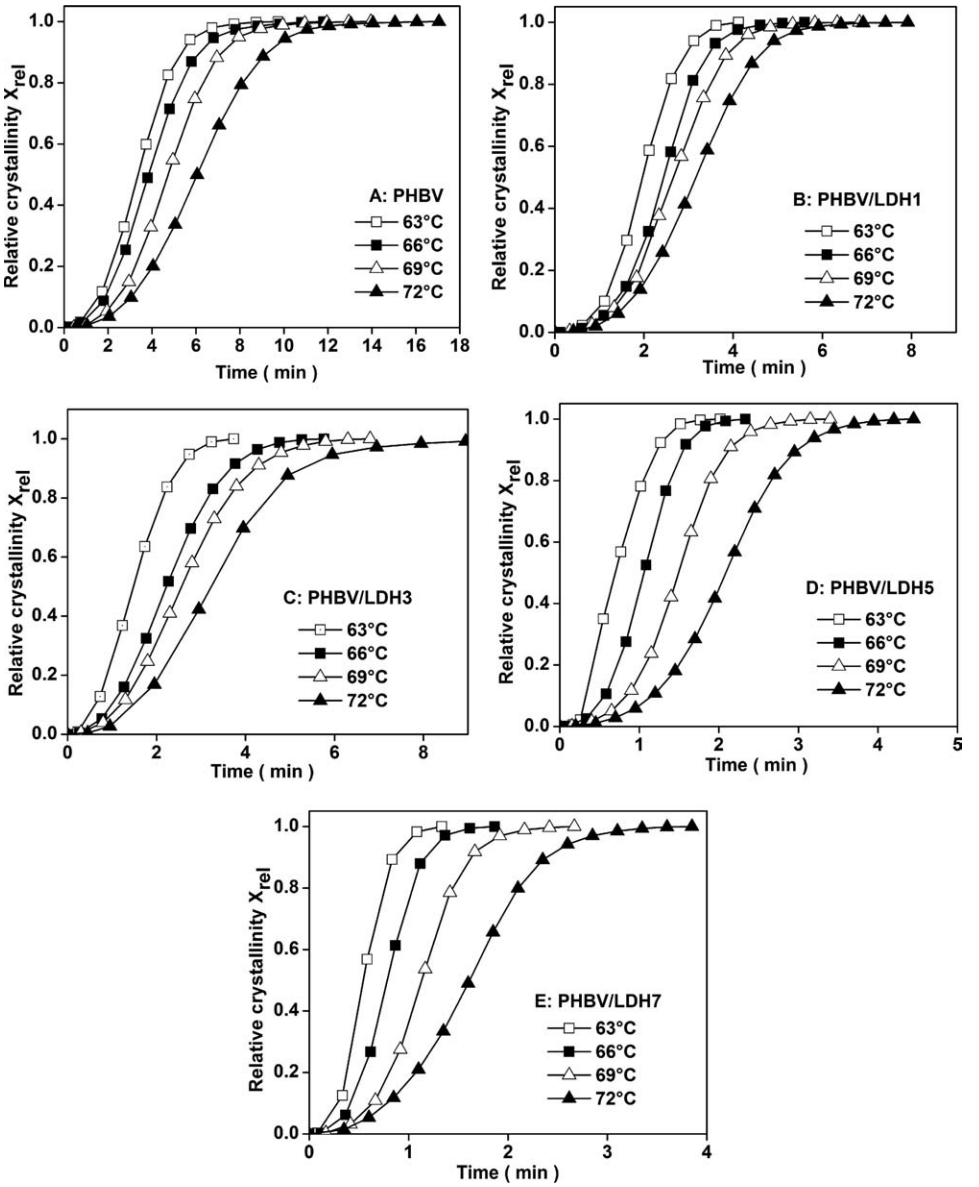

Figure 2. Plots of relative degree of crystallinity X_{rel} as a function of time at various T_c for PHBV and PHBV/LDH*n* nanocomposites.

$$X_{rel} = \frac{X_C(t)}{X_C(\infty)} = \int_0^t (dH/dt)dt \Big/ \int_0^\infty (dH/dt)dt \qquad (1)$$

The first integral is the heat of crystallization generated after time t and the second integral is the total heat of crystallization for $t = \infty$. X_{rel} is determined from the area under the exothermic peak in the DSC isothermal crystallization analysis at time t. Once the crystallization process is completed, the samples were reheated to 190°C at 10°C min^{-1} to examine the melting behavior. For all the samples, the crystallization temperatures investigated, T_cs, were selected to be in the vicinity of the peak of nonisothermal melt-recrystallization temperature (35–75°C).[21] T_cs investigated in this study are 63, 66, 69, and 72°C since they corresponded to the temperature range over, which an isothermal exothermic peak was obtained. All DSC measurements were performed and analyzed in duplicate.

Polarized Optical Microscopy Measurement

A Nikon POM equipped with an Instec STC200 hot-stage was used to investigate the super-structure of pure PHBV and its intercalated composites. Thin films (about 100 μm thick) were sandwiched between two thin glass slides and heated from 25 to 190°C at 50°C min^{-1}. The samples were then held at 190°C for 5 min. Subsequently, they were quenched to the appropriate T_c at 50°C min^{-1}. The samples were then held at T_c (35°C $\leq T_c \leq$ 125°C, 3°C increment) and the growth of spherulites as a function of time was monitored every minute for 5 min. With the aid of an interfaced video-camera, real-time spherulites growth measurements were performed. To minimize the thermal-

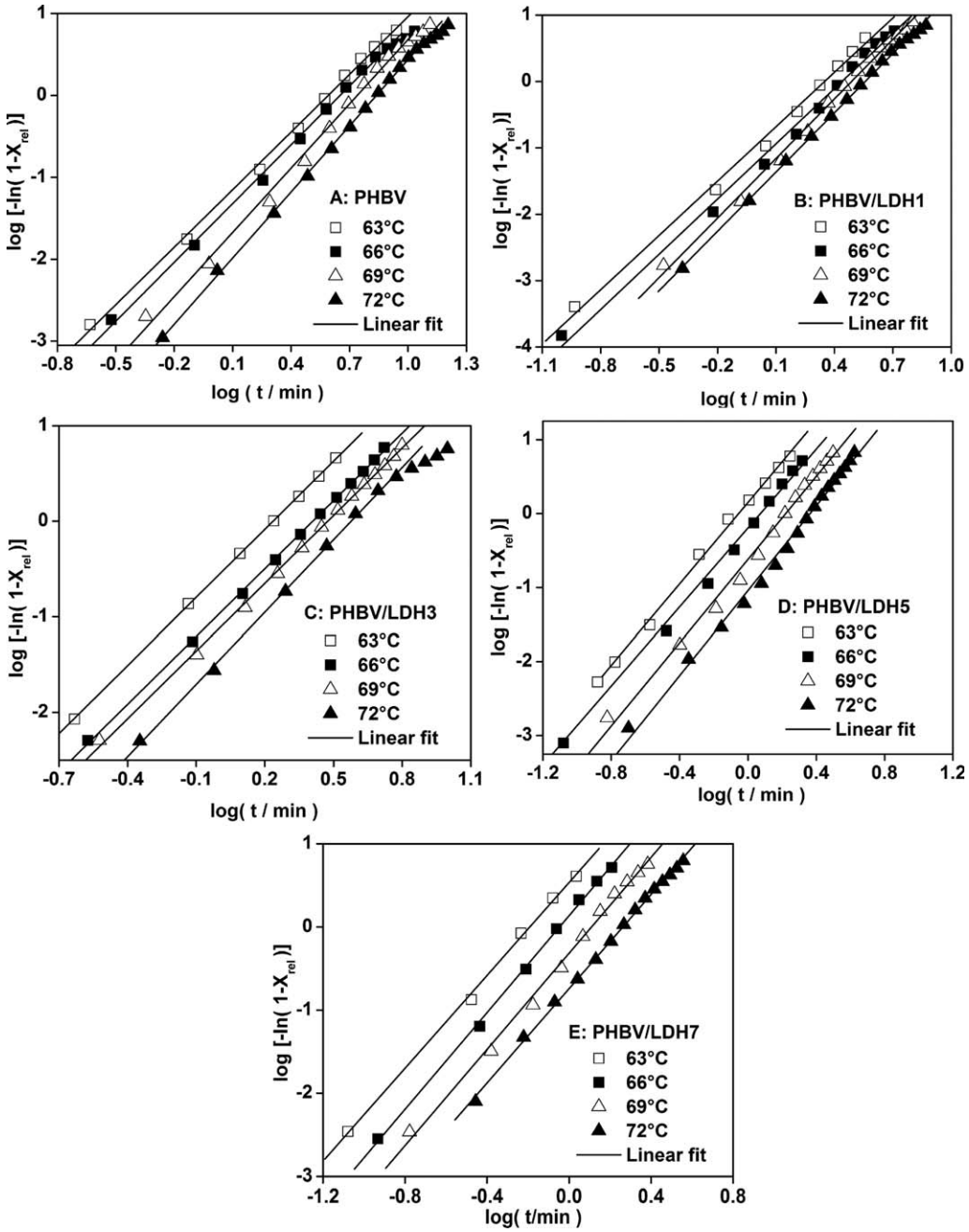

Figure 3. Plots of $\log[-\ln(1 - X_{rel})]$ as a function of $\log(t)$ at various T_c for PHBV and PHBV/LDH*n* nanocomposites.

degradation effects, a new sample was used for each crystallization measurement.

RESULTS AND DISCUSSION

Melting Behavior of PHBV by DSC

To evaluate the equilibrium-melting temperature T^0_m of PHBV and its nanocomposites, the effect of the cooling-thermal history on subsequent melting endotherms was determined. The melt-recrystallized PHBV and PHBV/LDH*n* nanocomposites samples were heated directly from T_cs after isothermal crystallization was performed. The thermograms of neat PHBV and PHBV nanocomposites samples displayed bimodal-melting endotherms (T_{m1} and T_{m2}). The two-peak behavior can be caused by a melt/recrystallization process.[11] For each sample, the authors observe that the higher-melting temperature peak, T_{m2}, is independent of T_cs, whereas the lower-temperature melting peak, T_{m1}, is dependent on the T_cs. It was postulated that T_{m2} is due to the melting of crystals that are recrystallized during heating of the samples in the DSC pans. On the other hand, T_{m1} is related to the melting of crystals formed during isothermal recrystallization from the melt.[13] For our study, T_{m1} and T_{m2} data plotted as a function of T_c are shown in Figure 1(A–E) for all samples. For each sample, T_{m1} increased gradually with increasing T_cs whereas T_{m2} is almost unchanged. The lower

Table I. Effect of LDH on the Avrami Exponent (n) and Crystallization Rate Constant (K_A), Activation Energy (E_A), and the Equilibrium Melting Temperature (T^0_m) of PHBV

Sample	T_c (°C)	$n \pm 0.10$	$K_A \pm 0.001$ (min^{-n})	$t_{1/2}$ (min)	E_A (kJ mol^{-1})	R^{2a}	$T^0{}_m$ (°C)
PHBV	63	2.34	0.041	3.348			
	66	2.39	0.028	3.829	−60.16 ± 2	0.98	187.7 ± 0.5
	69	2.62	0.012	4.703			
	72	2.69	0.005	6.255			
	63	2.83	0.111	1.956			
PHBV/LDH1	66	2.79	0.061	2.435	−72.23 ± 3	0.99	183.6 ± 0.4
	69	2.67	0.035	2.632			
	72	2.59	0.022	3.250			
	63	2.68	0.276	1.472			
PHBV/LDH3	66	2.68	0.107	2.207	−81.41 ± 5	0.99	180.4 ± 0.3
	69	2.56	0.076	2.558			
	72	2.45	0.035	3.195			
	63	2.59	1.391	0.782			
PHBV/LDH5	66	2.67	0.638	1.032	−99.48 ± 4	0.99	177.2 ± 0.4
	69	2.81	0.239	1.461			
	72	2.87	0.090	2.037			
	63	2.79	3.430	0.564			
PHBV/LDH7	66	2.91	1.370	0.791	−111.10 ± 5	0.99	171.3 ± 0.5
	69	2. 89	0.482	1.134			
	72	2.66	0.207	1.575			

[a]Regressional analysis for E_A determination.

of the two endothermic peaks is usually regarded as unstable and not a perfect crystal, whereas the higher is regarded as a stable and perfect one. Also, the trend in the melting temperatures is inversely related to the extent of crystal perfection. Our results show that the higher the content of LDH in PHBV matrix, the lower T_{m1} and T_{m2}.

Hoffman–Weeks technique[22] [eq. (2)] was used to estimate $T^0{}_m$ of crystals with infinite lamellar thickness of neat PHBV and PHBV in the nanocomposites. This equation describes the relation between T_{m1} and T_c,

$$T_m = T^0_{m1}\left[1 - \frac{1}{\gamma}\right] + \frac{T_c}{\gamma} \tag{2}$$

where $\gamma > 1$ and T^o_m is obtained from a plot of T_{m1} as a function of T_c by extrapolating the linear data until intersection with the $T_{m1} = T_c$ line. Figure 1(A–E) shows the plots of T_{m1} against T_c for all the samples. The extrapolated T^o_m value for PHBV is 187.7°C. This result is in good agreement with other studies.[14,23,24] T^o_m decreased with increasing LDH content. Indeed, it decreased from 187.7°C to 183.6, 180.4, 177.2, and 171.3°C corresponding to 1, 3, 5, and 7 wt % LDH, respectively. A similar result was reported by Hsu et al.[18] in their nanocomposites of P(3HB)/LDH nanocomposites. This result suggested that the crystalline structure of PHBV/LDHn nanocomposites was less perfect than that of neat PHBV. This behavior could result from the presence of more heterogeneous nucleation induced by the nanofiller and increased restriction of the biopolymer chains between the nanofiller, leading to a less perfect crystal causing $T_m{}^o$ to shift to lower temperatures.[18] This $T_m{}^o$ depression can allow processing of PHBV at lower melting temperature preventing its degradation. Thus, this characteristic enlarges the processing windows of PHBV.

Isothermal Crystallization Kinetics of PHBV by DSC

Crystallization of polymers, which involves nucleation and growth consecutively, is governed by both thermodynamics and kinetics considerations.[25] The presence of a solid surface in contact with a polymer melt usually results in heterogeneous nucleation. The isothermal crystallization kinetics of neat PHBV and PHBV in the nanocomposites can be analyzed by the Avrami model[26] according to eq. (3),

$$1 - X_{\text{rel}} = \exp(-K_A t^n) \tag{3}$$

where n (Avrami exponent) and K_A (Avrami isothermal crystallization rate constant) are determined by the mode of crystal nucleation and growth geometry under the experimental conditions. X_{rel} is the relative degree of crystallinity at time t defined in eq. (1) and t is the crystallization time. The plots of X_{rel} as a function of t are shown in Figure 2(A–E). The slopes of the curves at each point are a measure of the rate of crystallization. It can be observed that the rate of crystallization keeps constant for X_{rel} between 0.2 and 0.7 because those segments of the curves are almost straight. The deviation from the linearity starts at $X_{\text{rel}} = 0.7$, indicating that other factors such as secondary nucleation, exert influences at high conversions.

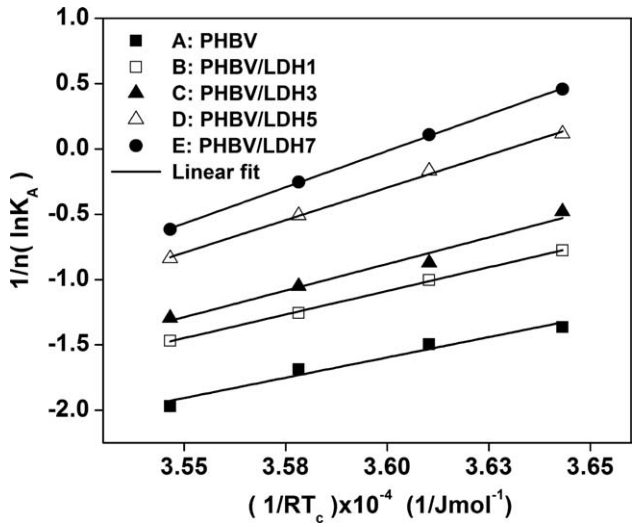

Figure 4. Arrhenius plots of $1/n$ (ln K) versus $1/RT_c$ for PHBV and PHBV/LDHn nanocomposites.

To utilize the Avrami model, the quantity $\log[-\ln(1 - X_{rel})]$ was plotted as a function of log t to obtain n and K_A. Since the Avrami equation is based on many assumptions such as linear crystal growth, primary nucleation, constant volume, and so forth, it is usually applicable at low conversions as long as impingement is not serious.[13] As a result, in this study n and K_A were calculated from the early linear segment of the Avrami plot. When $X_{rel} = 0.5$ in eq. (3), the half crystallization time, $t_{1/2}$, which is the time taken for the completion of 50% of "total volume" crystallization[13], is given by $t_{1/2} = (\ln 2/K_A)^{1/n}$. The Avrami plots of PHBV and its nanocomposites are shown in Figure 3(A–E) and the parameters n, K_A, and $t_{1/2}$ are given in Table I. From Figure 3(A–C), the authors note that for neat PHBV, PHBV/LDH1, and PHBV/LDH3 samples, the graphs at higher T_c show an initial linear segment during the early stage of crystallization and a tendency to level off due to the existence of secondary crystallization at a later stage.[15] This secondary crystallization is the result of slower crystallization, crystal perfection, and/or spherulites impingement in the later stage of the crystallization process. On the other hand, the upper segment of the graphs of PHBV/LDH5 [Figure 3(D)] and PHBV/LDH7 [Figure 3(E)] show almost a straight line. This indicates that at higher LDH content, the secondary crystallization in PHBV is reduced at higher T_cs. The Avrami exponent n varies in a narrow range, from 2.34 to 2.69 for neat PHBV, 2.59–2.83 for PHBV/LDH1, 2.45–2.68 for PHBV/LDH3, 2.67–2.87 for PHBV/ LDH5, and from 2.66 to 2.91 for PHBV/ LDH7. This illustrates that the crystal growth may not occur in three dimensions at an equal rate, and hence a low n value may be obtained. According to the Avrami model, in the ideal state of nucleated crystallization for three-dimensional crystallization growth, n had to be exactly 3.[15] However, in the actual process of crystal growth, the practical circumstances cannot satisfy the ideal state that the Avrami model is supposed to have; hence the deviation of the n value from 3. The nonintegral n value was reported by other authors[11,15,18] and may be considered because of the presence of mixed nucleation and growth mechanisms. Hence, these results indicate an athermal nucleation process followed by mixed three-dimensional and two-dimensional crystalline growth for PHBV and PHBV/LDHn nanocomposites, suggesting that the addition of LDH did not change the crystallization mechanism of PHBV.[18] For each sample, K_A increases with decreasing T_c, while $t_{1/2}$ increases with increasing T_c. These results indicated that with the increase of T_c, the crystallization rate decreases. K_A of PHBV/LDHn nanocomposites is much higher than that of the neat PHBV at the same T_c whereas $t_{1/2}$ is much lower, indicating a much faster crystallization rate in the nanocomposites. The addition of LDH into PHBV increases the rate of formation of crystalline phase. Also, K_A increases while $t_{1/2}$ decreases with increasing LDH content. These results indicate that the incorporation of LDH enhances the crystallization rate of PHBV and the large amount of the nanofiller is more effective than the small one. For example, $t_{1/2}$ of the neat PHBV at 63°C is 1.7, this is 2.3, 4.3, and 5.9 times as large as that of PHBV/LDH1, PHBV/LDH3, PHBV/LDH5, and PHBV/LDH7, respectively.

The crystallization process for PHBV and its nanocomposites is assumed to be thermally activated. Therefore, K_A can be approximately described by the following Arrhenius equation[18] to obtain the activation energy E_A [eq. (4)],

$$1/n(\ln K_A) = \ln K_0 - E_A/RT_C \quad (4)$$

where K_0, R, n, and T_c are the pre-exponential factor, universal gas constant (8.314 J $mol^{-1}K^{-1}$), Avrami exponent and the absolute crystallization temperature (Kelvin K), respectively. Plotting $1/n(\ln K_A)$ vs. $(RT_c)^{-1}$ (Figure 4), E_A can be obtained and its value for each sample is shown in Table I. The absolute magnitude of E_A increases with LDH content in PHBV matrix. The addition of LDH results both in the increased heterogeneous nucleation but more LDH induces more steric hindrance, thus reducing the transport of PHBV chains during crystallization.

Isothermal Crystallization Kinetics of PHBV by POM

The rate of isothermal crystallization from the melt of PHBV and its nanocomposite samples was also followed by a hot-stage optical microscopy. At the crystallization temperatures investigated (35°C $\leq T_c \leq$ 125°C), space-filling spherulites were observed to grow at a constant rate until their final impingement. Only large spherulites were observed in PHBV and PHBV/LDHn nanocomposites on crystallization. During the spherulites growth, the noncrystallizable LDH nanoparticles remain trapped in the interlamellar space, because their diffusion rate is much slower than the spherulite growth rate. It has been reported that the bacterial origin of PHBV determines its exceptional purity. It is precisely this purity that facilitates the growth of very large spherulites.[27,28] Figure 5(A–E) shows typical spherulitic superstructures of neat PHBV and PHBV/LDHn nanocomposites isothermally crystallized at 72°C. All the spherulites exhibit the characteristic of Maltese cross-section pattern. Another attractive aspect of the spherulites is the appearance of

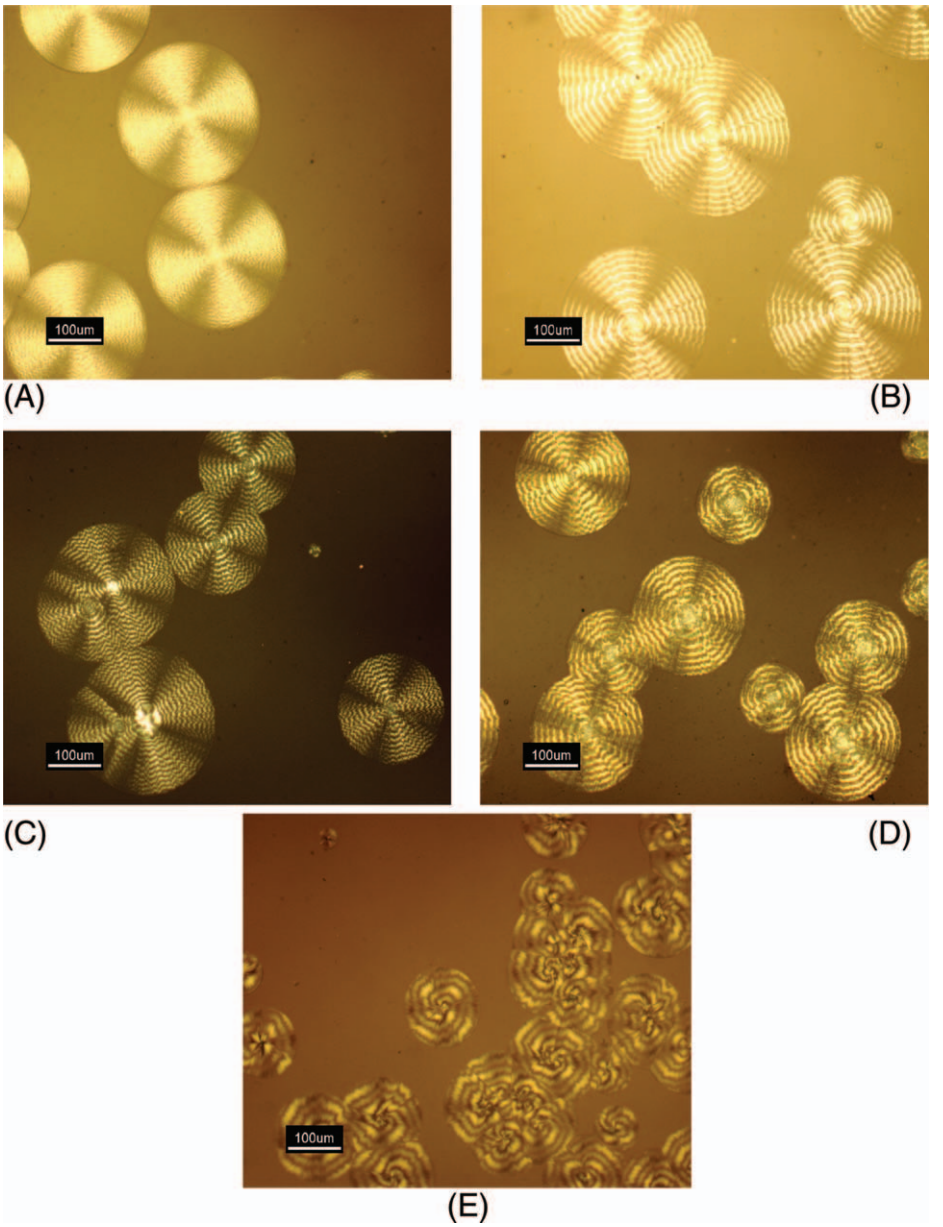

Figure 5. Polarized optical micrographs of (A) PHBV, (B) PHBV/LDH1, (C) PHBV/LDH3, (D) PHBV/LDH5, and (E) PHBV/LDH7 isothermally crystallized at 72°C. Scale bar: 100 μm. [Color figure can be viewed in the online issue, which is available at wileyonlinelibrary.com.]

defined "banding" extinction patterns. The extinction pattern exhibit double-ringed bands indicating a bi-axial optical character, expected for a polymer crystallizing with an orthorhombic structure.[27]

Spherulitic radial growth rates (G) of neat PHBV and its nanocomposites as a function of T_c were measured and reported in Figure 6. Bell-shaped curves were obtained, indicating the dependence of G on T_c. For neat PHBV, it can be seen that G has a maximum value at around 72°C. This value shifts to higher values with increasing LDH content (74°C for PHBV/LDH1, 77°C for PHBV/LDH3, 79°C for PHBV/LDH5, and 82°C for PHBV/LDH7), indicating the crystallization promoting effect of the nanofiller. The regime theory of polymer crystallization may be used to analyze G and obtain values for surface energies within crystals.[29] G may be described qualitatively by Turnbull and Fisher equation[30,31] [eq. (5)],

$$G = G_0 \exp\left[-\frac{\Delta E^*}{kT_C}\right] \exp\left[-\frac{\Delta F^*}{kT_C}\right] \quad (5)$$

where G_0 is a pre-exponential factor, k is Boltzmann constant equals to 1.38×10^{-23} J K^{-1}. The first term, exp $[-\Delta E^*/kT_c]$ describes the surface nucleation process in which ΔE^* is the free-energy of formation of a surface nucleus with critical size. The second term, exp $[-\Delta F^*/kT_c]$ is a molecular diffusion term in which ΔF^* is the free-energy for transporting molecular segments from the super-cooled phase to the crystalline phase. The

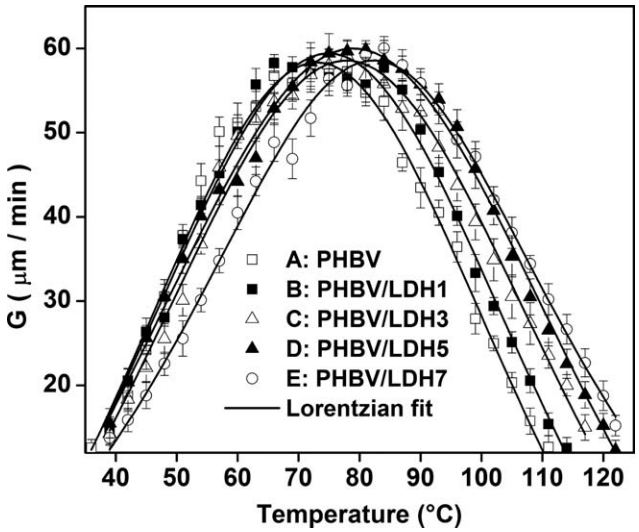

Figure 6. Spherulitic radial growth rates (G) as a function of crystallization temperature (T_c) for PHBV and PHBV/LDHn nanocomposites.

two terms are in opposition in the sense that as T_c is decreased, the first term decreases and the second increases, explaining the presence of a maximum in the behavior of G. The transporting term had to be dominant for the crystallization rate when T_c approaches the glass-transition temperature T_g, and the nucleation term had to be dominant when T_c approaches the melting temperature T_m. As shown in our previous study[21], PHBV exhibited T_g at 13°C and T_m at 170°C. In this study, T_c ranges from 35 to 125°C, where both the nucleation and transport processes control the crystallization rate.

On the basis of eq. (5) and to make the later equation compatible for the polymers crystallization in a large degree of supercoolings, Lauritzen–Hoffman theory[32] [eq. (6)] of secondary nucleation was used to analyze G data,

$$G = G_0 \exp\left[\frac{-U^*}{R(T_c - T_\infty)}\right] \exp\left[-\frac{K_g}{fT_c\Delta T}\right] \quad (6)$$

where G_0 is a growth-rate constant that is essentially temperature independent, U^* is the activation energy for the transport of crystallizable segments to the crystal front through the subcooled melt, R is the gas constant, T_∞ is the temperature below, which segmental motions cease, $\Delta T = T_m^0 - T_c$ the degree of supercooling, where T_m^0 is the equilibrium melting point and T_c is the crystallization temperature. The correction factor f for the temperature dependence of the equilibrium enthalpy of melting is equal to $2T_c/(T_m^o + T_c)$. K_g the nucleation parameter representing the free-energy required to form a nucleus of critical size can be expressed by eq. (7),

$$K_g = \left[\frac{\beta b_0 \sigma \sigma_e T_m^0}{k\Delta H_m^0}\right] \quad (7)$$

where b_0 is the molecular layer thickness, σ and σ_e are the lateral and fold surface free-energy of the growing crystals, respectively, k, the Boltzmann constant, and ΔH_m^o the enthalpy of melting of perfect crystal. The parameter β is related to the characteristic of the crystallization growth and may have the value of 2 or 4. Hoffman proposes that there are three distinct regimes (I, II, and III) of growth of polymer crystals, depending on the relative rates of formation of new secondary nuclei on the growth front and the rate at which, the nuclei once formed spread along the growth front. At low supercoolings (high T_c), the rate of spreading is so large when compared with that of nucleation that a nucleus once formed spreads right across the growth front. This is referred to as regime I and corresponds to $\beta = 4$. At high supercoolings (low T_c), several nuclei form and spread across the front together, the separation between them decreasing as supercooling increases. This is referred to as regime II and leads to $\beta = 2$. If crystallization occurs at still much higher supercoolings (much lower T_c), the separation between the multiple nuclei characteristic of regime II reaches its minimum value. This is regime III and leads to $\beta = 4$.

To analyze the growth kinetics of PHBV spherulites in the framework of Lauritzen–Hoffman theory [eq. (6)], the quantity $\ln G + U^*/R(T_c - T_\infty)$ was plotted as a function of $1/fT_c\Delta T$.[33,34] to obtain K_g (slope) and G_0 (intercept). U^* and T_∞ need to be estimated and were varied to maximize the correlation coefficient. T_m^0 values are listed in Table I. The best fit for PHBV, shown in Figure 7A, was obtained using $U^* = 10.25$ kJ mol^{-1} and $T_\infty = 258$ K, which is T_g-30 K. The most notable feature on the PHBV plot is that all the growth rate data (covering a crystallization temperature range from 35 to 125°C) fall on a single line. This meant that no regime transition was shown for 35 to 125°C. Similar result was obtained by Organ and Barham[29] and Pen et al.[30]. They identified the transition from regime II to regime III around 130–140°C. Therefore, our data for T_c range studied (35–125°C) for PHBV can be attributed to regime III. For PHBV, The values of K_g and G_0 extracted from the fitted plot were 4.03×10^5 K^2 and 36,879 cm s^{-1}, respectively (Table II). Peng et al.[30] investigated the isothermal crystallization

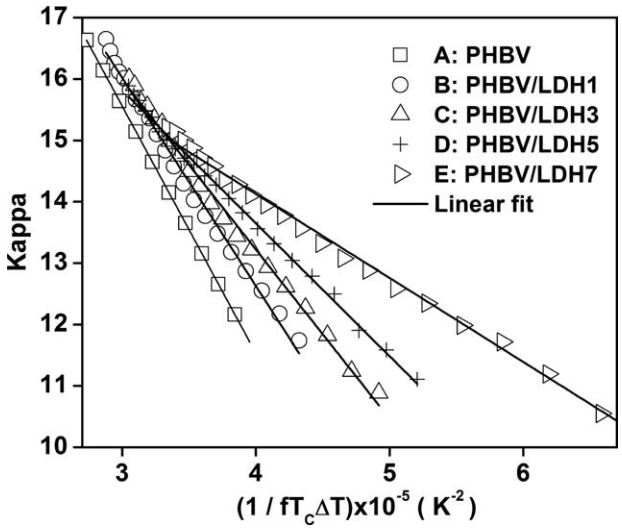

Figure 7. Plot of kappa versus $1/(fT_C\Delta T)$ for PHBV and PHBV/LDHn nanocomposites: Kappa = $\ln G + [U^*/R(T_C - T_\infty)] - \ln \varphi_2[1 + (2\sigma T_m^0/fb_0\Delta H_m^0\Delta T)]$. For neat PHBV, $\varphi_2 = 1$.

Table II. Effect of LDH on the Crystallization Temperature (T_c) at G_{max}, Nucleation Constant (K_g), Growth Rate Constant (G_0), Fold Surface Energy (σ_e), and Work of Chain Folding (Q) of PHBV

Sample	T_C at G_{max} (°C)	$K_g \times 10^5$ (K^2)	R^{2a}	G_0 (cm s^{-1})	σ_e (erg cm^{-2})	$\sigma\sigma_e$ (erg^2 cm^{-4})	$Q \times 10^{13}$ (erg)
PHBV	72.0	4.03 ± 0.37	0.998	36879	32.91	855.66	1.26
PHBV/LDH1	74.0	3.39 ± 0.25	0.997	22026	27.90	725.40	1.07
PHBV/LDH3	77.0	2.76 ± 0.15	0.998	13359	22.87	594.62	0.88
PHBV/LDH5	79.0	2.15 ± 0.08	0.998	9996	17.94	466.44	0.69
PHBV/LDH7	82.0	1.38 ± 0.03	0.997	4914	11.67	303.42	0.45

[a]Regressional analysis for K_g determination.

behavior by POM between 75 and 115°C of PHBV. Their K_g obtained from a regime III was found to be 3.14×10^5 K^2.

To confirm to which regime, the growth rate data in selected T_c range belong to, the authors applied the Lauritzen Z[35] test using eq. (8),

$$Z = 10^3 \left(\frac{L}{2a_0}\right)^2 \exp\left[-\frac{X}{T_C \Delta T}\right] \quad (8)$$

where L is the effective lamellar thickness and a_0 is the molecular layer width in the crystal. The procedure consists in using eq. (8) to calculate L values. According to this test, if the substitution of $X = K_g$ into the test results in $Z \leq 0.01$, regime I or III kinetics are followed. On the other hand, if $X = 2K_g$ into the test yields $Z \geq 1.0$, regime II kinetics are followed. As pointed out by Lauritzen and Hoffman, it is more convenient to use a known value of K_g and the inequalities for Z to obtain L values in regime I, II, or III and to estimate if such values are realistic. Kunioka et al.[8] studied the crystalline structure of PHBV and found that for the 3-HV content up to 37 mol%, the crystal lattice of PHBV is the same as that of PHB. Therefore, the unit cells of PHBV (18 mol% 3-HV content) investigated in our work can be considered orthorhombic (space group $P2_12_12_1$) with $a = 5.8$ Å, b = 13.2 Å and c (fiber axis) = 5.96 Å.[8] The values of the molecular layer width a_0 and thickness b_0 are equal to 6.6 and 5.8 Å, respectively.[30] Assuming $Z \geq 1.0$ and substituting $X = 2K_g$ into the test, $L \geq 3.5 \times 10^4$ Å, which is clearly high and impossible. Hence, regime II can be eliminated. Assuming $Z \leq 0.01$ and substituting $X = K_g$ into the test, $L \leq 12.5$ Å, and this calculation is reasonable for PHBV. This calculation confirmed that the crystallization regime to be regime III, and the parameter $\beta = 4$ can be adopted.

In view of the analysis of PHBV spherulitic growth rates in the presence of LDH, additional terms must be added to account for the nanofiller presence,[14,36] and consequentially eq. (6) must be adapted. For polymer–diluent system, eq. (6) was modified by Boon and Azcue[37] to obtain eq. (9) to describe G of a crystallizable polymer in a single-phase melt containing a diluent.

$$G = \varphi_2 G_0 \exp\left[\frac{-U^*}{R(T_c - T_\infty)}\right] \exp\left[\left(-\frac{K_g}{fT_c\Delta T}\right) + \left(\frac{2\sigma T_m^0 \ln \varphi_2}{fb_0 \Delta H_m^0 \Delta T}\right)\right] \quad (9)$$

In this article, the pre-exponential factor G_0 is multiplied by φ_2 (weight fraction of crystallizable polymer) to account for the dilution due to the nanofiller because the rate of nucleation is proportional to the content of the polymer-crystallizable units. The additional term in the second exponential is an entropic contribution to the free-energy of activation for nucleus formation, which accounts for the probability of selecting the required number of crystallizable polymer sequences from the mixture at the given φ_2. To utilize eq. (9), the quantity Kappa defined as $\ln G + [U^*/R(T_C - T_\infty)] - \ln\varphi_2[1 + (2\sigma T_m^0/fb_0\Delta H_m^0\Delta T)]$ was plotted as a function of $1/fT_c\Delta T$ to obtain K_g and G_0 for PHBV/LDH*n* nanocomposites (the authors note that for the analysis of neat PHBV spherulitic growth rates in a single melt without diluent, φ_2 is equal to 100% = 1, thus Kappa = $\ln G + [U^*/R(T_C - T_\infty)]$). $\Delta H^0{}_m$ of 100% crystalline PHBV was not measured directly, but was taken from published reports and is equal to 1.65×10^8 J m^{-3}.[30] As for neat PHBV, the best fit for PHBV/LDH*n* nanocomposite samples, shown in Figure 7B–E, was obtained using $U^* = 10.25$ kJ mol^{-1}, $T_\infty = 258$ K and $T_m{}^0$ values listed in Table I. For each nanocomposite sample, the growth rate data fall on the single line as in the case for neat PHBV. The derived K_g and G_0 values for each nanocomposite sample were listed in Table II. In our study, the authors observe that K_g and G_0 decrease with increasing the content of the nanofiller. This result meant that the presence of LDH in PHBV matrix led to a decrease in the energy barrier for secondary nucleation. In the same method as for neat PHBV, the authors conducted Lauritzen Z test on the PHBV/LDH*n* nanocomposite samples and concluded that their crystallization belonged to the regime III too.

The lateral surface energy σ of the developing crystals can be calculated using the relation suggested by Lauritzen and Hoffman[38] [eq. (10)] based on Thomas–Staveley relation,[39]

$$\sigma = \alpha_{LH} \Delta H_m^0 (a_0 b_0)^{1/2} \quad (10)$$

where α_{LM} is an empirically determined constant and is equal to 0.25 for high-melting polyesters, a_0b_0 is the cross-sectional area of the PHBV chain.[38] Our calculated value of σ is 2.6×10^{-2} J m^{-2}, which is 26 erg cm^{-2}.

The derived K_g [eq. (7)] can be used to calculate the fold surface energy σ_e for PHBV and its nanocomposites Table II summarized σ_e and the product $\sigma\sigma_e$. The value of σ_e for neat PHBV is 32.91 erg cm^{-2}. The authors observe that σ_e decreased with

increasing LDH content. In general, the smaller σ_e, the faster the crystallization rate of polymer crystal. In PHBV/LDH*n* nanocomposites, σ_e decreased with increasing LDH content indicating that the incorporation of LDH into PHBV may induce the heterogeneous nucleation of PHBV crystallization and then decrease the surface-energy barrier for PHBV crystallization. The result showed that the conclusion based on Lauritzen–Hoffman theory is consistent with that of Avrami model. Finally, the different σ_e values of PHBV and its nanocomposites correspond to the work of chain folding, Q, given by the following relation [eq. (11)].[30]

$$Q = 2a_0b_0\sigma_e \tag{11}$$

The values of Q are given in Table II. Q obtained for neat PHBV is 1.26×10^{13} erg per molecular chain fold. The authors observed that the value of Q decreased with increasing LDH content. This decrease could have meant that PHBV in the nanocomposites will take less energy than the neat PHBV to yield fold-chain crystals, indicating the crystallization promoting effect of LDH.

CONCLUSION

PHBV/LDH*n* nanocomposites containing randomly intercalated LDH within the PHBV matrix have been successfully prepared through solution route. The authors have previously shown that the DSC nonisothermal crystallization from the melt indicated that the parent PHBV lacked a melt-recrystallization peak T_{mc}.[21] With the addition of LDH, T_{mc} appeared and shifted to higher-crystallization temperature with increasing the content of the nanofiller.[21] The above-fact indicated a crystallization promoting effect of LDH in PHBV. To explore in detail, the crystallization behavior of PHBV, the Avrami model, and Lauritzen–Hoffman theory were used. Isothermal crystallization results from DSC measurements showed that the addition of the nanofiller induced more heterogeneous nucleation in the crystallization significantly increasing the crystallization rate and the absolute magnitude of the activation energy ΔE_A. Hoffman–Weeks plots were used to estimate the equilibrium melting points $T^0{}_m$ of PHBV and its nanocomposites. In neat, PHBV, $T^0{}_m$ was 187.7 $\pm$ 0.5°C. Increasing the content of LDH in the PHBV matrix resulted in lowering the equilibrium melting point after isothermal crystallization. The value of Avrami exponent n = 2.34–2.91 illustrated that crystal growth may not occur in three dimensions at an equal rate and the addition of LDH did not change the mechanism of nucleation and growth of PHBV. The experimental data of spherulitic growth rate were analyzed according to the polymer-diluent theory based on Lauritzen–Hoffman model. The results indicated regime III crystallization for PHBV and PHBV/LDH*n* nanocomposites. The nucleation constant K_g, the folded-surface energy σ_e and the work of chain folding Q of PHBV crystals are 4.03×10^5 K^2, 32.91 $\pm$ 0.04 erg cm^{-2} and 1.26×10^{13} erg, respectively. These values decreased with increasing LDH content and suggested that the incorporation of LDH into PHBV induced heterogeneous nucleation of the biopolymer crystallization and decreased the surface energy barrier for PHBV crystallization.

ACKNOWLEDGMENTS

We acknowledge the support of Lucia Innocenti-Mei in providing us with PHBV, Paul Braterman in guiding us on LDH synthesis and the UNT-Center for Advanced Research and Technology (CART), for instrumentation training.

REFERENCES

1. Bordes, P.; Pollet, E; Avérous, L. *Prog. Polym. Sci.* **2009,** *34*, 125.
2. Paul, D. R.; Robeson, L. M. *Polymer* **2008,** *49*, 3187.
3. Anderson, A. J.; Dawes, E. A. *Microbiol. Rev.* **1990,** *54*, 450.
4. Philip, S.; Keshavarz, T.; Roy, I. *J. Chem. Technol. Biotechnol.* **2007,** *82*, 233.
5. Lee, Y. H.; Kang, M. S.; Jung, Y. M. *J. Biosci. Bioeng.* **2000,** *89*, 380.
6. Miao, L.; Qiu, Z.; Yang, W.; Ikehara, T. *React. Funct. Polym.* **2008,** *68*, 446.
7. Kunioka, M.; Doi, Y. *Macromolecules* **1990,** *23*, 1933.
8. Kunioka, M.; Tamaki, A.; Doi, Y. *Macromolecules* **1989,** *22*, 694.
9. Holmes, P. A. *Phys. Technol.* **1985,** *16*, 32.
10. Bhardwaj, R.; Mohanty, K. A.; Drzal, L. T.; Pourboghrat, F.; Misra M. *Biomacromolecules* **2006,** *7*, 2044.
11. Ma, P. M.; Wang, R. Y.; Wang, S. F.; Zhang, Y.; Zhang, Y. X.; Hristova, D. *J. Appl. Polym. Sci.* **2008,** *108*, 1770.
12. Bruzeau, S.; Bourmaud, A. *Polym. Test.* **2007,** *26*, 652.
13. Qian, J.; Zhu, L.; Zhang, J.; Whitehouse, R. S. *J. Polym. Sci. B: Polym. Phys.* **2007,** *45*, 1564.
14. Chen, G. X.; Hao, G. J.; Guo, T. Y.; Song, M. D.; Zhang, B. H. *J. Appl. Polym. Sci.* **2004,** *93*, 655.
15. Kai, W.; He, H.; Inoue, H. *Polym. Int.* **2005,** *54*, 780.
16. Braterman, P. S.; Xu, Z. P.; Yarberry, F. In Handbook of Layered Materials, Auerbach S. M., Carrado, K. A., Dutta, P. K., Eds.; Marcel Dekker: New York, **2004, 373.**
17. Dagnon, K. L.; Ambadapadi, S.; Shaito, A.; Ogbomo, S. M.; DeLeon, V.; Golden, T. D.; Rahimi, M.; Nguyen, K.; Braterman P. S.; D'Souza, N. A. *J. Appl. Polym. Sci.* **2009,** *113*, 1905.
18. Hsu, S. F.; Wu, T. M.; Liao, C. S. *J. Polym. Sci. B: Polym. Phys.* **2006,** *44*, 3337.
19. Pucciariello, R.; Tammaro, L.; Villani, V.; Vittoria, V. *J. Polym. Sci. B: Polym. Phys.* **2007,** *45*, 945.
20. Chen, W.; Feng, L.; Qu, B. *Chem. Mater.* **2004,** *16*, 368.
21. Dagnon, K. L.; Chen, H. H.; Innocentini-Mei, L. H.; D'Souza, N. A. *Polym. Int.* **2009,** *58*, 133.
22. Hoffman, J. D.; Weeks, J. J. *J. Chem. Phys.* **1962,** *37*, 1723.
23. Liu, W. J.; Yang, H. L.; Wang, Z.; Dong, L.; Liu, J. J. *J. Appl. Polym. Sci.* **2002,** *86*, 2145.
24. Akhtar, S.; Pouton, C. W.; Notarianni, L. J. *Polymer* **1992,** *33*, 117.
25. Yang, J.; McCoy, B. J.; Madras, G. *J. Chem. Phys.* **2005,** *122*, 1.

26. Avrami, M. *J. Chem. Phys.* **1940,** *8*, 212.
27. Lovera, D.; Márquez, L.; Balsamo, V.; Taddei, A.; Castelli, C.; Müller, A. *J. Macromol. Chem. Phys.* **2007,** *208*, 924.
28. Barham, P. J.; Keller, A.; Otun, E. L.; Holmes, P. A. *J. Mater. Sci.* **1984,** *19*, 2781.
29. Organ, S. J.; Barham, P. J. *J. Mater. Sci.* **1991,** *26*, 1368.
30. Peng, S.; An, Y.; Chen, C.; Fei, B.; Zhuang, Y.; Dong, L. *Eur. Polym. J.* **2003,** *39*, 1475.
31. Turnbull, D.; Fischer, J. C. *J. Chem. Phys.* **1949,** *17*, 71.
32. Lauritzen, J. I.; Hoffman J. D. *J. Appl. Phys.* **1973,** *44*, 4340.
33. Hoffman, J. D.; Davis, G. T.; Lauritzen, J. I. Jr. In Treatise on Solid State Chemistry; Hannay, N. B., Ed.; Plenum Press: New York, **1976;** Vol.*3*, Chapter 7.
34. Hoffman, J. D. *Polymer* **1983,** *24*, 3.
35. Lauritzen, J. I. *J. Appl. Phys.* **1973,** *44*, 4353.
36. Pizzoli, M.; Scandola, M.; Ceccorulli, G. *Macromolecules* **2002,** *35*, 3937.
37. Boon, J.; Azcue, J. M. *J. Polym. Sci. A-2* **1968,** *6*, 885.
38. Hoffman, J. D.; Miller, R. L.; Marand, H.; Roitman, D. B. *Macromolecules* **1992,** *25*, 2221.
39. Thomas, D. G.; Staveley L. A. K. *J. Chem. Soc.* **1952, 4569.**